Scientific Reports

https://doi.org/10.1038/s41598-026-40507-5

Article in Press

High sensitivity formalin detection in aqueous solutions using plasmonic multifunctional metal insulator metal nanoring based optical refractive index sensor platform

Received: 29 April 2025

Accepted: 13 February 2026

Published online: 22 February 2026

Cite this article as: Khodaie A., Rafighirani Y., Heidarzadeh H. *et al.* High sensitivity formalin detection in aqueous solutions using plasmonic multifunctional metal insulator metal nanoring based optical refractive index sensor platform. *Sci Rep* (2026). https://doi.org/10.1038/s41598-026-40507-5

Ali Khodaie, Yousef Rafighirani, Hamid Heidarzadeh, Javad Javidan & Yesudasu Vasimalla

High Sensitivity Formalin Detection in Aqueous Solutions Using Plasmonic Multifunctional Metal Insulator Metal Nanoring Based Optical Refractive Index Sensor Platform

Ali Khodaie [1], Yousef Rafighirani [1], Hamid Heidarzadeh [1,*], Javad Javidan [1], Yesudasu Vasimalla[2]

[1] Department of Electrical and Computer Engineering, University of Mohaghegh Ardabili, Ardabil, Iran.

[2]Centre of Excellence for Nanotechnology, Department of Electronics and Communication Engineering, Koneru Lakshmaiah Education Foundation, Vaddeswaram, Vijayawada, Andhra Pradesh, 522302, India.

*Corresponding author: heidarzadeh@uma.ac.ir

Abstract

Formalin contamination in water poses major health and environmental risks, requiring rapid and sensitive detection. This study presents a plasmonic optical biosensor refractive index sensor based on a multifunctional metal–insulator–metal (MIM) nanoring structure optimized for formalin detection. The proposed design features nested nanorings with perpendicular arms and **a** reflective metal layer, **e**nabling strong electromagnetic confinement and multi-resonance operation and multi-resonance operation. Finite-difference time-domain simulations demonstrate four resonance modes with sensitivities of 1289.30, 823.31, 662.71, and 557.62 nm/RIU, and corresponding FOM values up to 13.73 RIU^{-1}. The sensor exhibits a linear spectral shift versus refractive index variation of aqueous formalin (n = 1.3300–1.3600). Electric-field analysis confirms field localization at resonant sites, contributing to enhanced sensing performance. These results demonstrate the potential of the proposed MIM nanoring platform for highly sensitive and compact optical sensing applications, particularly in real-time environmental monitoring of hazardous chemicals.

Keywords: optical biosensor, sensitivity, formalin, multifunctional, metal-insulator-metal nanorings.

1. Introduction

The detection of hazardous chemicals in environmental and biological systems has become a critical priority in modern science, driven by increasing concerns over public health and safety. Among these chemicals, formaldehyde (commonly encountered as formalin in aqueous solutions) poses a significant threat due to its widespread use and inherent toxicity. Formaldehyde is a volatile organic compound employed extensively in industrial processes, construction materials, and as a preservative in food and medical applications [1]. However, its classification as **a** Group 1 human carcinogen by the International Agency for Research on Cancer underscores the urgent need for effective monitoring solutions. Prolonged exposure to formaldehyde is linked to severe health issues, including respiratory disorders, nasopharyngeal cancer, and myeloid leukemia [3]. Occupational studies further reveal that workers in high-exposure industries exhibit a higher incidence of respiratory symptoms and diminished lung function compared to those with minimal exposure [4]. Given its pervasive presence and associated risks, the development of rapid, sensitive, and cost-effective detection methods for formalin in aqueous environments is paramount. Traditional analytical techniques for formalin detection, such as ion chromatography (IC), high-performance liquid chromatography (HPLC), and gas chromatography (GC), have long been regarded as gold standards due to their precision and reliability [5]. Ion chromatography separates charged particles based on their electrical properties, offering robust detection capabilities, while HPLC excels in analyzing polar compounds with high resolution [6]. Gas chromatography, which is particularly suited for volatile organic compounds like formaldehyde, provides exceptional sensitivity but requires meticulous sample preparation and costly equipment [7]. Despite their effectiveness, these methods suffer from significant drawbacks, including operational complexity, the need for highly purified reagents, and frequent equipment maintenance [8]. Additionally, spectrophotometric approaches, while simpler and more accessible, often lack the sensitivity and specificity required for complex matrices, as interfering substances can skew results [9]. These limitations highlight the necessity for innovative alternatives that combine ease of use with high performance, particularly for real-time, on-site applications in environmental monitoring and food safety.

In recent years, there has been a notable surge in research on plasmonic devices, driven by their exceptional capability to control light at the nanoscale. This area has seen exploration across a broad spectrum of applications, such as oxidation resistance devices [10], inverse photonic structures [11], nanoantennas [12], optical demultiplexers [13,14], interferometric setups [15], optical couplers [16,17], computing-oriented logic gates [18], and a variety of highly sensitive sensors [19]. The goal of these investigations is to leverage the remarkable optical characteristics of surface plasmons to create compact, high-speed, and energy-efficient photonic components for emerging technologies. The advent of nanotechnology and plasmonic biosensors has revolutionized sensing, offering promising solutions to the shortcomings of conventional methods. These include metamaterial-based ring resonator [20], chemical sensors [21], magnetic field sensors [22], flow sensors [23], as well as pressure [24] and temperature sensors [25,26]. Such sensors are designed to offer enhanced sensitivity, miniaturization, and rapid response times for advanced sensing applications. Plasmonic sensors, which leverage surface plasmon resonance (SPR), have gained attention for their label-free detection, high sensitivity to refractive index changes, and real-time monitoring capabilities [27]. The emergence of metal-insulator-metal (MIM) configurations, enabled by metamaterials, has further advanced this field by providing compact, efficient platforms for optical sensing [28]. Metamaterials, characterized by their subwavelength structures and unique electromagnetic properties such as negative permittivity and permeability, enhance the interaction between light and matter, making them ideal for constructing plasmonic biosensors [29].

Among the metals commonly used, gold, silver, and aluminum stand out due to their excellent plasmonic properties, with silver being particularly favored for its chemical stability and strong SPR response [30]. These materials, when paired with dielectric substrates like silicon dioxide (SiO_2), enable the design of multifunctional optical biosensors capable of detecting minute changes in their surrounding environment. The motivation for this work stems from the need to address the limitations of existing plasmonic sensors, such as intrinsic losses and manufacturing defects, which can compromise performance [31]. Metals in plasmonic systems experience ohmic heating, reducing the strength of localized electric fields and thus impacting biosensing efficacy. Additionally, imperfections like surface roughness or misalignment during fabrication increase scattering losses, leading to discrepancies between theoretical and experimental outcomes [32]. By optimizing the geometric dimensions of the MIM nanoring structure and carefully selecting materials, this study seeks to mitigate these challenges, enhancing the sensor's efficiency for practical applications. The incorporation of back reflectors further amplifies the electromagnetic response, improving the sensor's ability to detect subtle changes in the refractive index induced by formalin presence.

The proposed biosensor is analyzed using the FDTD method, a powerful numerical tool for solving Maxwell's equations and simulating electromagnetic behavior [33]. This approach allows for precise evaluation of the sensor's reflection spectrum, sensitivity, and figure of merit (FOM), critical metrics for assessing its performance. The design's versatility extends beyond formalin detection, with potential applications in medical diagnostics, such as virus detection, when integrated with microfluidic systems [34]. By combining the strengths of plasmonic MIM nanorings with advanced fabrication techniques like electron beam lithography and nanoimprint lithography, this study aims to deliver a robust, scalable platform for real-time chemical sensing. The present study proposes a multifunctional plasmonic optical biosensor based on MIM nano-ring structures that incorporates gold, silver, and aluminum as plasmonic materials and SiO_2 as a dielectric substrate. The design features nested nanorings with backing reflectors made of gold, silver, or aluminum, which aims to increase the sensitivity and ability to detect formalin and other analytes.

2. Structure and method

2.1. Background and materials

Recent advances in metamaterials have enabled the design of highly efficient MIM nanoring structures composed of subwavelength metallic elements [35]. These engineered materials exhibit strong electromagnetic responses and unique optical properties, including negative permittivity and permeability, making them highly suitable for plasmonic biosensing applications. Among various materials, gold, silver, and aluminum are considered the most important materials for building these structures [36]. In this study, gold, silver, and aluminum are used as to create a plasmonic multifunctional optical biosensor based on MIM nanorings. The insulating dielectric substrate is made of a layer of SiO_2. Additionally, to enhance the performance of the structure, three different back reflectors are incorporated, one made of gold and the other made of silver and aluminum. The optical properties of gold, silver, aluminum, and SiO_2 are derived from the data provided by Palik [30]. MIM-based nanoring structures offer a compact and efficient platform for optical sensing, demonstrating improved performance compared to conventional plasmonic sensors. As a result, they have attracted significant research interest in recent years. In this study, we present a multifunctional plasmonic biosensor based on nested MIM nanorings, and describe its physical configuration and dimensional parameters in detail. The design typically features one or more metal rings, which can take various geometric forms, such as squares or circles, with silver being the preferred material for the nanorings in the optimized design. When these nanorings are exposed to a time-varying magnetic field, an annular electric current is induced, generating a magnetic dipole moment perpendicular to the nanoring.

2.2. Design mechanism

Figure 1 shows the structural design, which consists of two nanorings paired with two perpendicular arms. This configuration is intentionally selected to boost the sensor's overall performance. The nanorings are placed on a glass substrate in a nested layout, where one ring has a radius of R and the other has a radius of 1.4R. The parameter Wr represents the width of both the rings and the arms, d denotes the arm length, and hr indicates the thickness of these components. The structure also includes a dielectric layer beneath the nanorings, defined by side length L and thickness hd. To further improve sensing capability, a reflective layer is positioned under the dielectric layer with thickness hb. Together, these material and geometric parameters are examined to achieve optimal sensor performance, with the final optimized dimensions listed in Table 1. Plasmonic systems, however, are highly sensitive to losses and fabrication imperfections. Metals used as plasmonic materials inherently suffer from ohmic losses, which weaken the generated local electric fields and limit their effectiveness in biosensing. The magnitude of these losses depends on the material properties. Fabrication imperfections also pose difficulties; structural irregularities can increase scattering losses and diminish device efficiency. For example, surface roughness can intensify scattering at metal interfaces, while dimensional inaccuracies or misalignments can create discrepancies between simulated and measured behavior. By refining geometric design, selecting appropriate materials, and enhancing fabrication techniques, plasmonic devices can achieve higher efficiency and broader applicability across advanced technological fields [37].

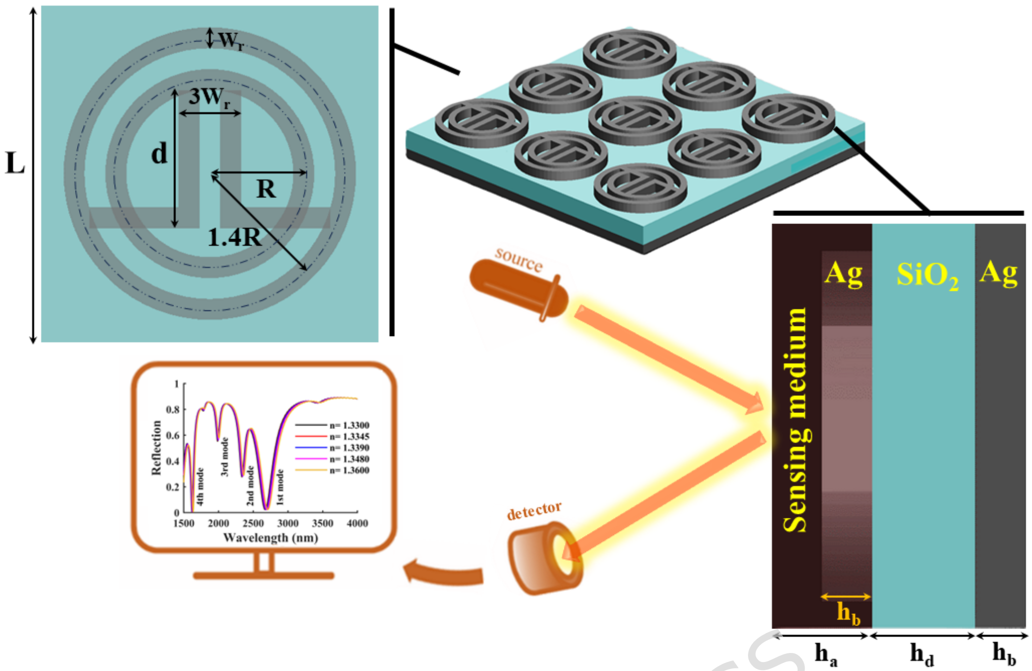

Figure 1 Schematic diagram of the proposed plasmonic multifunctional metal-insulator-metal (MIM) nanoring-based optical biosensor, featuring nested nanorings, perpendicular arms, a dielectric substrate, and a back reflector.

Table 1 Dimensional parameters of the sensor after optimization.

Parameter	Symbol	Value
Dielectric length	L	1300 nm
radius of the inner ring	R	360 nm
Arm length	d	540 nm
Rings and arms width	W_r	80 nm
Back Reflector thickness	h_b	80 nm
Dielectric thickness	h_d	150 nm
Rings and arms thickness	h_r	80 nm
Analyte thickness	h_a	200 nm

2.3. Analysis method

The proposed system is analyzed using the FDTD numerical method, where Maxwell's equations are solved through the Yee algorithm. For this purpose, the commercially available Lumerical FDTD analyzer, widely used in optics, photonics, and nanoelectronics, is employed. In the FDTD method, the mesh is set as auto-non-uniform, with the "Conformal '0' mode" applied to modify it. Mesh accuracy is set to '10', and a separate mesh with dx=dy=dz= 2 nm is used in the structure-sensitive regions of the MIM nanorings. The refractive index of the background is set to that of air, which is 1. The simulation time is fixed at 1000 fs with a temperature of 300 K, utilizing the Field Time monitor. Perfectly matched layer (PML) boundary conditions are applied along the z-axis, while periodic boundary conditions are used in the x and y directions. Light is sourced from a flat wave, with wavelengths ranging from 1500 to 4000 nm, in TE polarization mode. This range covers the near-infrared (NIR) to mid-infrared (MIR) regions, where many plasmonic and dielectric materials such as silicon, germanium, and certain chalcogenides show strong, tunable resonant behavior with relatively low optical losses and high refractive indices. Moreover, the MIR region is particularly valuable for sensing because many molecules exhibit distinct vibrational and absorption features in this part of the spectrum. The reflection spectrum is analyzed using the Frequency-domain field and power monitor, and the distribution of the electromagnetic field is visualized with the Frequency-domain field profile monitor.

2.4. Performance criteria

To assess sensor performance, including sensitivity and FOM, an analyte layer can be placed on the MIM nanoring structure. Adjusting the refractive index of the analyte (Δn_s) results in a shift in the reflection spectrum at the resonance wavelength ($\Delta\lambda_0$). The sensor's sensitivity is expressed in nanometers per refractive index unit (nm/RIU), which represents the shift of the resonance wavelength relative to a change in the refractive index of the analyte [38]:

$$S = \frac{\Delta\lambda_0}{\Delta n_s} \qquad [\mathrm{nm \cdot RIU^{-1}}] \qquad (1)$$

The FOM is a quantitative metric used to evaluate and compare the overall performance of an optical sensor. It consolidates multiple performance parameters, such as sensitivity and response time, into a single value that simplifies comparative analysis among sensors or technologies. The sensor's FOM can be mathematically expressed as follows. The sensor's FOM is calculated in terms the inverse refractive index unit (RIU^{-1}), which divides the sensitivity (S) by the FWHM and indicates the resonant quality of the sensor [39]:

$$FOM = \frac{S}{FWHM} \qquad [RIU^{-1}] \tag{2}$$

Here, FWHM represents the full width at half maximum, which is an essential parameter in optical sensor technology. FWHM characterizes the quality of the resonances in the reflection spectrum and provides valuable insight into the sensor's overall quality and sensitivity. A smaller FWHM is preferred as it indicates better resolution in detecting the resonance of biological samples.

Additionally, the lowest measurable value that the sensor can detect is known as the Limit of Detection (LoD), Here , FWHM (in nanometers), and $\Delta\lambda_0$ is the resonance wavelength shift (in nanometers). The LoD is calculated as the minimum detectable change in refractive index (in RIU) [40]:

$$LoD = \left(\frac{\Delta n_s}{1.5}\right) \times \left(\frac{FWHM}{\Delta\lambda_0}\right)^{1.25} \qquad [RIU] \tag{3}$$

It should be noted that the reported LoD values are theoretical estimates derived from the simulation-based resonance shift and FWHM, and actual LoD performance may vary in practical experiments due to fabrication tolerances and measurement noise; therefore, experimental validation will be required to accurately confirm the sensor's real-world detection limit.

When designing a sensor, minimizing material consumption and device size is crucial, particularly in compact and resource-efficient applications. For instance, enlarging the sensor's cavity might improve sensitivity but would also require a larger volume of analyte, conflicting with the goal of miniaturization. To address this trade-off, we propose a new performance metric called the sensitivity-to-volume ratio (SVR), which evaluates how effectively a sensor balances sensitivity with its physical footprint. SVR is mathematically defined as the ratio of sensitivity to sensor volume. The SVR is calculated in nanometers to the negative power of two per unit of refractive index $\left(\frac{1}{nm^2 RIU}\right)$, which divides the sensitivity by the total sensor volume [25]:

$$SVR = \frac{S}{V} \qquad [nm^{-2} \cdot RIU^{-1}] \qquad (4)$$

Where, S represents the sensor's sensitivity, while V denotes its total volume. Our proposed biosensor achieves an optimal SVR of 2.461×10^{-6} $nm^{-2}.RIU^{-1}$ in 1st mode, demonstrating an efficient balance between high detection capability and compact design. This metric highlights the sensor's ability to deliver strong performance while minimizing its physical footprint.

3. Results and Discussion

3.1. Optimization of structural materials

This section presents the outcomes of the theoretical analysis of the proposed plasmonic multifunctional optical biosensor based on metal-insulator-metal (MIM) nanorings, focusing on its performance in detecting formalin in aqueous environments. The results, derived from FDTD simulations, elucidate the effects of material choice (gold, silver, and aluminum) and structural parameters on reflectance spectra, sensitivity, and FOM. The discussion interprets these findings in the context of plasmonic losses, fabrication feasibility, and comparative performance against existing sensors, highlighting the design’s potential for real-time environmental monitoring applications.

Figure 2 evaluates the performance of plasmonic optical sensor using different materials (gold, silver, and aluminum) for the back reflector and nanorings across four resonance modes, presented through six subfigures (a–f). Subfigures (a) and (b) display the reflectance spectra for the back reflector and nanorings, respectively, over a wavelength range of 1500 to 4000 nm, highlighting material-specific plasmonic resonances. Silver and aluminum exhibit sharper peaks compared to gold, indicating stronger light interaction. Subfigures (c) and (d) compare the sensitivity (nm/RIU) for the back reflector and nanorings, with silver demonstrating the highest sensitivity, particularly in higher resonance modes, enhancing the sensor's ability to detect minute refractive index changes. Subfigures (e) and (f) assess the FOM for both components, where silver achieves superior values, reaching up to 13.73 RIU^{-1} in the fourth mode for nanorings, reflecting improved precision and resolution. These findings affirm silver as the optimal material for high-precision sensing applications, such as pollutant detection, offering a pathway to more effective environmental monitoring solutions. Figure 2 compares the sensitivity and figure of merit (FOM) for different materials (silver, gold, and aluminium) across four resonance modes. Silver exhibits high sensitivity in the 1st mode (1289.30 nm/RIU), suitable for detecting large refractive index changes, while aluminium provides a higher FOM in the 4th mode (13.73 RIU^{-1} compared to 12.95 RIU^{-1} for silver), indicating better resolution for trace detection. The minimal differences between materials suggest that the optimal material choice depends on the specific application requirements, such as prioritizing sensitivity or resolution.

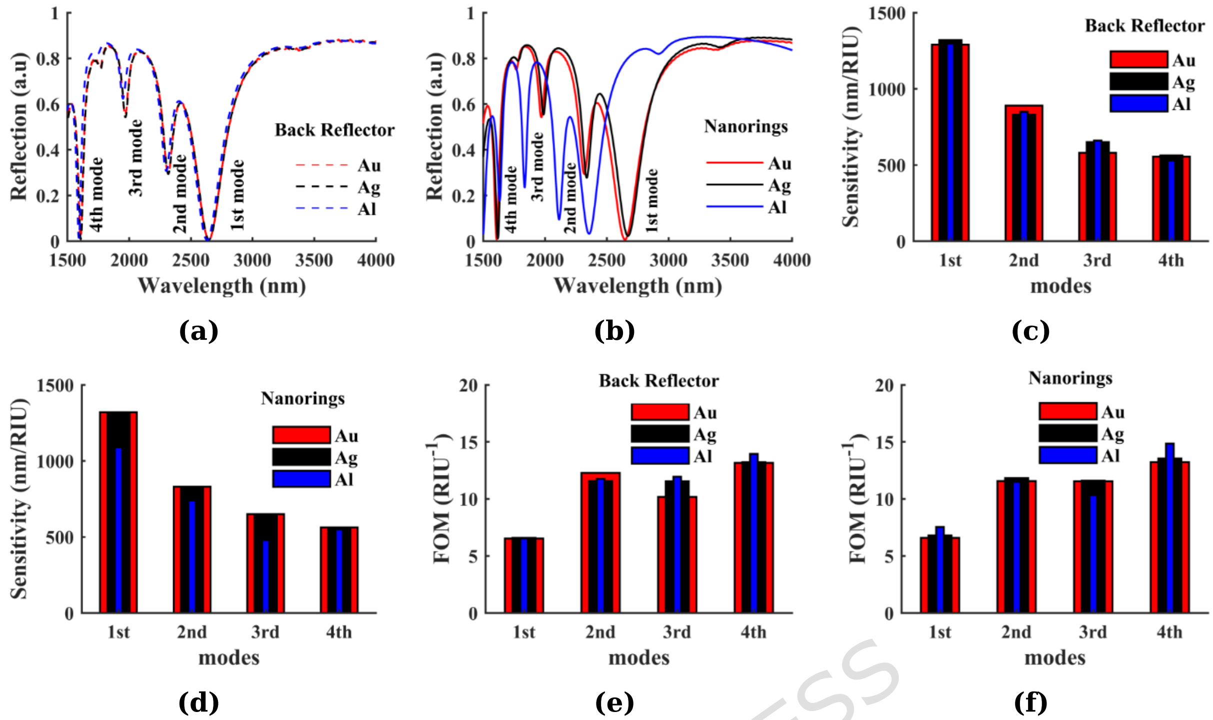

Figure 2 (a, b) Reflectance spectra, **(c, d)** Sensitivity, and **(e, f)** FOM of the proposed biosensor for different materials (gold, silver, and aluminum) used in the back reflector and nanorings, respectively, across four resonance modes.

3.2. Geometry optimization of the structure

Figure 3 investigates the performance of the plasmonic optical sensor by analyzing the impact of thickness variations in the back reflector (h_b) and nanorings (h_r) across four resonance modes, presented through six subfigures (a–f). Subfigures (a) and (b) depict the reflectance spectra for the back reflector and nanorings, respectively, within a wavelength range of 1500 to 4000 nm, using thicknesses of 75, 80, 85, and 90 nm for the back reflector, and 65, 70, 75, 80 nm for nanorings. These spectra reveal shifts in plasmonic resonances, with peaks shifting to higher wavelengths as thickness increases. Subfigures (c) and (d) evaluate the sensitivity for the back reflector and nanorings, demonstrating that a thickness of 80 nm yields the highest sensitivity (up to 1290 nm/RIU) for both components, enhancing the sensor's capability to detect minute refractive index changes. Subfigures (e) and (f) compare the FOM for both elements, where a thickness of 80 nm again outperforms others, achieving FOM values up to 14 RIU^{-1} in the fourth mode for nanorings, thereby improving precision and resolution. These findings highlight that optimizing the thickness of the back reflector and nanorings at 80 nm significantly enhances the sensor’s performance, paving the way for more accurate environmental monitoring applications.

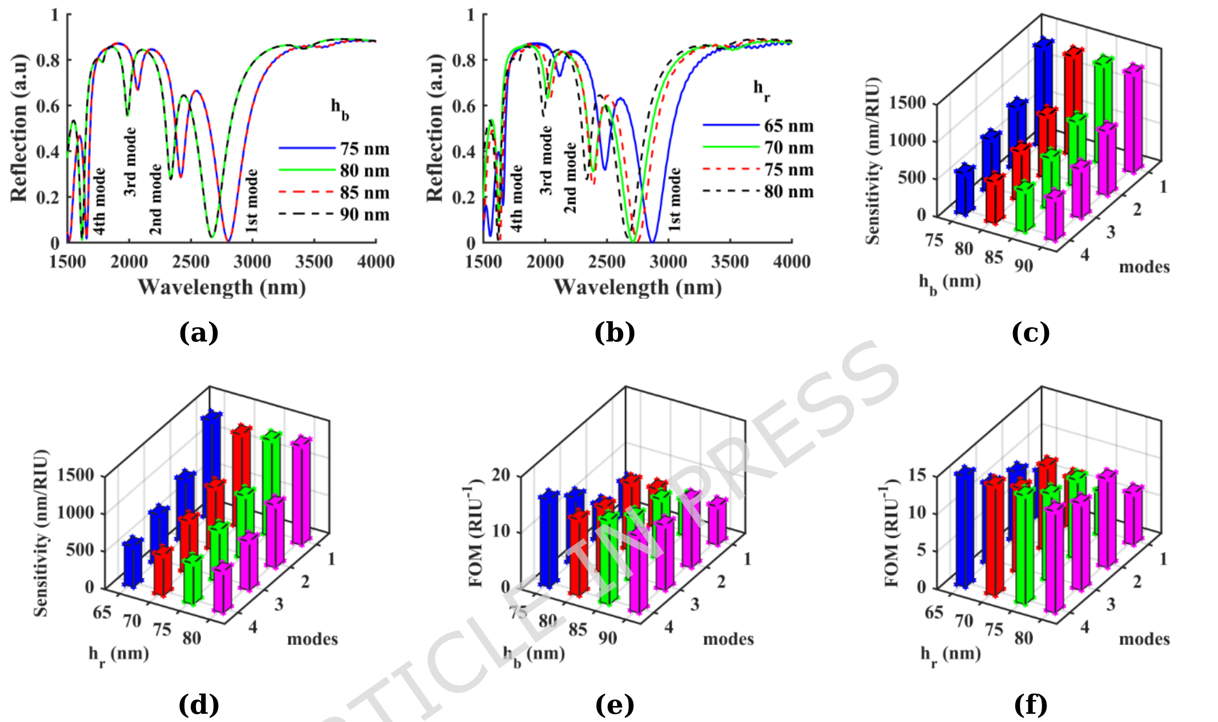

Figure 3 (a, b) Reflectance spectra, **(c, d)** Sensitivity, and **(e, f)** FOM of the proposed structure versus changes in the thickness of the back reflector (h_b) and nanorings (h_r), respectively, in all four resonance modes.

3.3. Electric field distribution of the structure

Figure 4 illustrates the proposed MIM nanoring-based plasmonic biosensor's electric field (E-field) distribution across four resonance modes, simulated using the FDTD method with Lumerical FDTD analyzer. Subfigures (a–d) represent the 1st to 4th resonance modes, respectively, showing the spatial distribution and intensity within the structure (x- and y-axes ranging from -650 to 650 nm), with inner (R = 360 nm) and outer (1.4R = 504 nm) radii of the nested nanorings. The color bar on each subfigure indicates the E-field intensity in arbitrary units (a.u.), with scales varying per mode. Figure 4(a) depicts the 1st mode with an intensity range of 0 to 20 a.u., showing a symmetric field concentrated along the inner edges of the nanorings, with peak intensity (~20 a.u.) at the inner and outer ring edges (bright red regions). Figure 4 (b) shows the 2nd mode (0 to 10 a.u.), with the field focused along the perpendicular arms and inner ring edges (~10 a.u.). Figure 4 (c) presents the 3rd mode (0 to 6 a.u.), with the field localized at nanoring-arm intersections (~6 a.u.). Figure 4 (d) illustrates the 4th mode (0 to 15 a.u.), with highly confined fields at the same intersections (~15 a.u.). The figure reveals the evolution of field distribution, from broad and intense in the 1st mode (highest sensitivity, 1289.30 nm/RIU) to more localized in higher modes, with the 4th mode achieving the highest FOM (13.73 RIU^{-1}), optimizing the sensor's performance for formalin detection. To increase physical clarity, the dispersion relation of the MIM nanoring structure was presented using the surface plasmon model, and the origin of the four resonant modes, the field localization behavior, and their distribution differences were qualitatively explained. This semi-analytical discussion helps to better understand the resonant behavior.

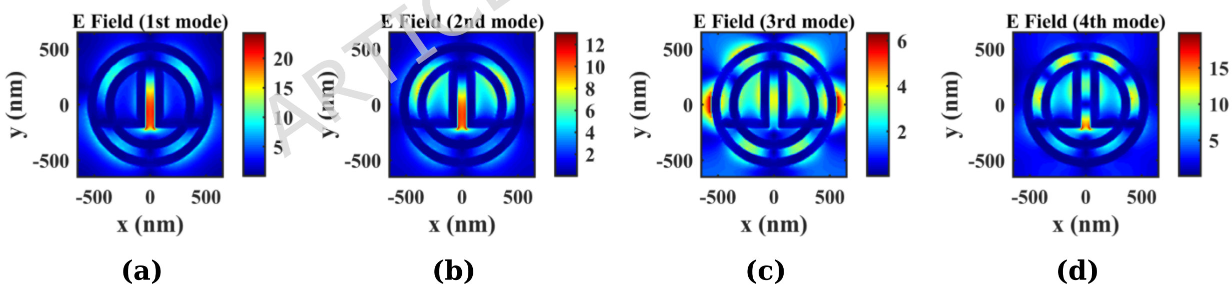

Figure 4 Distribution of the electric field (E/E_0) in the proposed biosensor for the **(a)** first, **(b)** second, **(c)** third, and **(d)** fourth resonance modes.

3.4. Formalin Detection in Aqueous Solutions

Figure 5 explores how the MIM nanoring-based plasmonic biosensor responds to changes in the refractive index (n) of formalin in water, varying from 1.3300 to 1.3600, which corresponds to different formalin concentrations. The figure includes six parts (a–f), created using FDTD simulations across a wavelength range of 1500 to 4000 nm. Parts (a) to (e) show the reflection spectra for four resonance modes, while part (f) illustrates the linear relationship between the resonance wavelength shift (Δλ) and the refractive index change (Δn). This analysis reveals how the sensor detects formalin through shifts in resonance wavelength, a key technique in plasmonic biosensing with practical uses in environmental monitoring and pollutant detection.

Figure 5 (a) presents the reflection spectra for all four resonance modes at refractive indices of 1.3300, 1.3345, 1.3390, 1.3480, and 1.3600. The horizontal axis covers wavelengths from 1500 to 4000 nm, and the vertical axis shows reflectance from 0 to 1. At n = 1.3300, four distinct resonance dips appear: the 1st mode at ~2670 nm, 2nd mode at ~2330 nm, 3rd mode at ~1980 nm, and 4th mode at ~1610 nm. As n increases to 1.3600, these dips shift to ~2710 nm, ~2362 nm, ~2007 nm, and ~1635 nm, respectively, showing a clear shift. The 1st mode exhibits the largest shift (~50 nm), matching its high sensitivity of 1289.30 nm/RIU. This shift happens because the plasmonic field interacts strongly with the formalin, turning small environmental changes into measurable wavelength shifts. Figure 5 (b) zooms in on the 4th resonance mode, with the horizontal axis ranging from 1550 to 1750 nm and the vertical axis from 0 to 1. At n = 1.3300, the resonance dip is at 1618.5 nm. As n increases to 1.3345, 1.3390, 1.3480, and 1.3600, the dip moves to 1620 nm, 1623 nm, 1628 nm, and 1635 nm, respectively. This mode has a sensitivity of 557.6 nm/RIU, an FWHM of 40.62 nm, and an FOM of 13.73 RIU^{-1}, showing it can detect tiny amounts of formalin with great clarity, perfect for real-world tasks like checking water quality. Figure 5 (c) focuses on the 3rd resonance mode, with the horizontal axis from 1900 to 2100 nm and the vertical axis from 0 to 1. At n = 1.3300, the dip is at 1987 nm, shifting to 1989 nm, 1993 nm, 1999 nm, and 2007 nm as n increases to 1.3345, 1.3390, 1.3480, and 1.3600, respectively. The sensitivity here is 662.7 nm/RIU, with an FWHM of 56.09 nm and an FOM of 11.81 RIU^{-1}, offering a good balance of sensitivity and clarity for quick and accurate detection. Figure 5 (d) highlights the 2nd resonance mode, with the horizontal axis from 2250 to 2450 nm and the vertical axis from 0 to 1. The dip at n = 1.3300 is at 2330 nm, moving to 2341 nm, 2345 nm, 2353 nm, and 2362 nm as n increases. This mode has a sensitivity of 823.3 nm/RIU, an FWHM of 70.1 nm, and an FOM of 11.73 RIU^{-1}, making it great for tasks needing higher sensitivity, like detecting small changes in formalin levels.

Figure 5 (e) shows the 1st resonance mode, with the horizontal axis from 2500 to 3000 nm and the vertical axis from 0 to 1. At n = 1.3300, the dip is at 2671 nm, shifting to 2677 nm, 2683.5 nm, 2694 nm, and 2710 nm as n increases. The sensitivity is 1289.3 nm/RIU, with an FWHM of 193.7 nm and an FOM of 6.65 RIU^{-1}. This mode has the highest sensitivity, making it ideal for detecting larger changes, though its broader FWHM slightly lowers its clarity. Figure 5 (f) plots the resonance wavelength shift (Δλ) against the refractive index change (Δn) (from 0 to 0.03) for all four modes, with the horizontal axis (Δn) from 0 to 0.03 and the vertical axis (Δλ) from 0 to 60 nm. Linear fits are provided: 1st mode (y = 1289.3x + 0.24169), 2nd mode (y = 823.31x + 0.017326), 3rd mode (y = 662.71x + 0.02134), and 4th mode (y = 557.62x + 0.030874). These lines match the sensitivities in Table 2, confirming the sensor's consistent performance. The 1st mode shows the largest shift, while the 4th mode shows the smallest, reflecting how each mode interacts differently with the formalin. Figure 5 demonstrates the sensor's ability to detect formalin through wavelength shifts. The 1st mode, with a sensitivity of 1289.30 nm/RIU and a 50 nm shift (for Δn = 0.03), excels at detecting larger changes, while the 4th mode, with an FWHM of 40.62 nm and an FOM of 13.73 RIU^{-1}, offers the best clarity. This versatility across modes makes the sensor a powerful tool for environmental monitoring, such as detecting water contamination in industrial or lab settings, ensuring safer and cleaner environments.

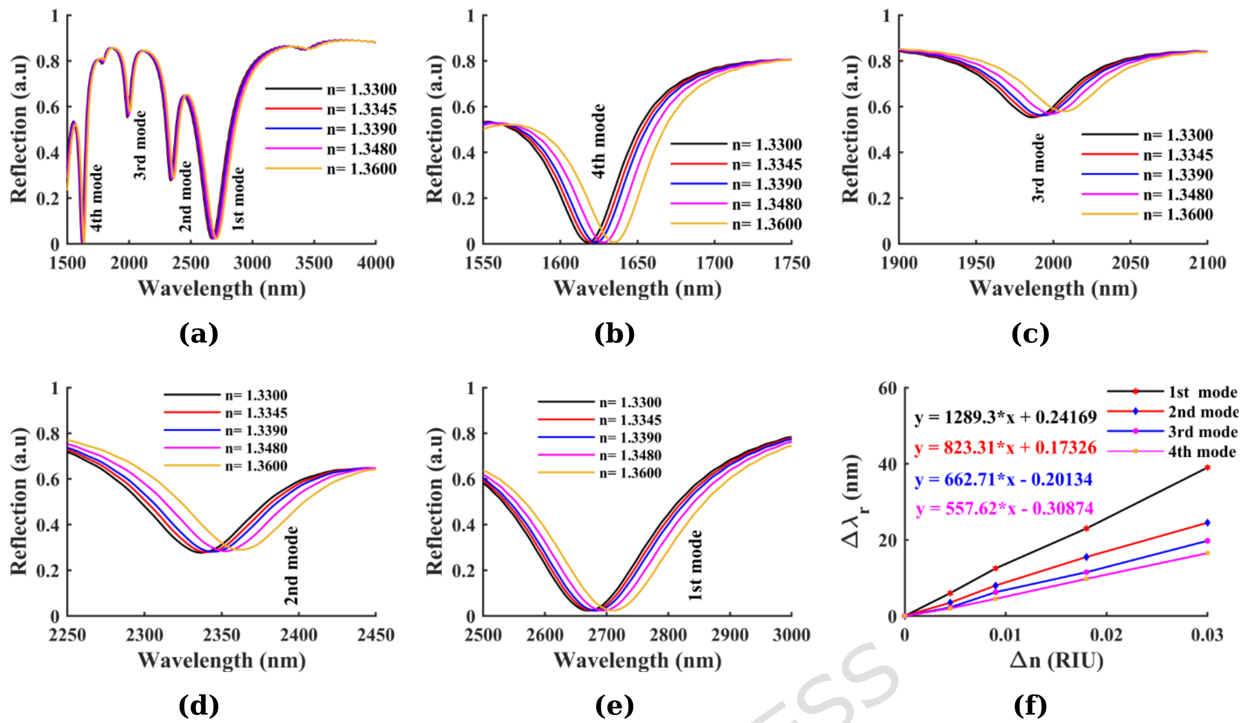

Figure 5 **(a)** Overview of reflection spectra for formalin refractive index variations (*1.33 to 1.36*). **(b–e)** Detailed spectral shifts for the first through fourth resonance modes. **(f)** Linear regression of resonance wavelength shift (Δλ) versus refractive index change (Δn).

3.5. Performance comparison and fabrication methods

Table 2 provides a comprehensive comparison of the performance parameters of the proposed plasmonic optical sensor across four resonance modes with previously reported works, focusing on key metrics such as sensitivity, FWHM, FOM, and LoD. The comparison aims to highlight the superior capabilities of the proposed sensor for plasmonic sensing applications, particularly in detecting minute changes in the refractive index. Compared to previous works, the proposed sensor consistently outperforms most references in terms of sensitivity, particularly in the first mode (1289.30 nm/RIU). Additionally, the FOM in the fourth mode (13.73) marks a notable improvement over many prior studies, highlighting the sensor's enhanced precision for applications like pollutant detection or medical monitoring. The LoD values, ranging from 0.127 to 0.230, further confirm the sensor's capability to detect low analyte concentrations, a critical factor for practical applications. This analysis underscores the proposed sensor's ability to achieve an optimal balance of sensitivity, precision, and detection limits, positioning it as a promising candidate for advanced sensing technologies in environmental and healthcare domains.

The 1st mode of the sensor, with a sensitivity of 1289.30 nm/RIU, excels in detecting large refractive index changes, ideal for applications like higher formalin concentration detection. However, its higher FWHM (193.79 nm) results in lower resolution and a reduced FOM (6.65 RIU^{-1}) compared to the 4th mode (FOM of 13.73 RIU^{-1}, FWHM of 40.62 nm), which is optimized for high-resolution detection of trace formalin amounts. This trade-off between sensitivity and resolution highlights the sensor's versatility for diverse environmental and medical applications.

Moreover, to fabricate the proposed sensor, there are different deposition techniques are available such as, Physical Vapor Deposition (PVD), and Chemical Vapor Deposition (CVD), which have certain draw backs like non-conformity in coating and uniformity. Alternatively, if the atomic layer deposition (ALD) technique is used, we can ensure conformal deposition of Ag and SiO_2 layers, which will have uniform thickness and enhanced adhesion on the prism surface. Also, precise thickness of layers can be achieved using ALD than others as the coating occurs in an atomic level with high accuracy. While ALD offers excellent control over film thickness and uniformity making it ideal for precise nanofabrication it is true that its relatively high cost and lower throughput compared to other deposition methods can pose challenges for large-scale manufacturing. However, recent advancements in spatial ALD and batch processing techniques have significantly improved throughput and reduced per-unit cost, making the process increasingly viable for commercial applications.

Table 2 Comparison of performance parameters of four resonance modes of the proposed structure with previously reported works.

References	configuration	application	λ range	RI range	polarization	sensitivity (nm/RIU)	FWHM (nm)	FOM (RIU^{-1})	LoD (RIU)
41	MIM waveguide	cancer cell	1000-2000	1.3-1.6	TE	1200	---	---	---
42	nano-rings	Cancer cell	750-1000	1.333-1.368	TE	524.3	52.3	10	---
43	nano-particles	glucose/fructose	950-1200	1.333-1.354	TE	584.9	52	11.22	---
44	microring resonator	general	1500-1600	1.334-1.342	TE	403	---	---	---
45	PC-waveguide	general	1350-1380	2.998-3.002	TE	308	---	---	---
46	Patterned Plasmonic	general	650-900	---	---	225	---	---	---
47	metamaterial	general	100-300	1.35-1.44	TE	300	---	---	---
48	MIM nano-discs	SARS-CoV-2	300-1000	1.35-1.491	TE	313	39.1	4	---
This work (1st mode)			2500-3000	1.33-1.36	TE	1289.30	193.79	6.65	0.230
This work (2nd mode)			2250-2500	1.33-1.36	TE	823.31	70.19	11.73	0.127
This work (3rd mode)			1900-2100	1.33-1.36	TE	662.71	56.09	11.81	0.167
This work (4th mode)			1500-1750	1.33-1.36	TE	557.62	40.62	13.73	0.129

Conclusion

This study investigated an MIM nanoring-based plasmonic optical sensor for detecting formalin in aqueous environments. FDTD simulations demonstrated its performance across four resonance modes. Reflection spectra confirmed linear wavelength shifts with refractive index changes (n) from 1.3300 to 1.3600, achieving sensitivities of 1289.30 nm/RIU (1st mode), 823.31 nm/RIU (2nd mode), 662.71 nm/RIU (3rd mode), and 557.62 nm/RIU (4th mode). The 1st mode notably outperformed prior studies, which reported. The 4th mode offered high resolution with an FOM of 13.73 RIU^{-1} and an FWHM of 40.62 nm, while the 1st mode, with an FWHM of 193.7 nm and an FOM of 6.65 RIU^{-1}, provided superior sensitivity. Electric field distribution revealed that the 1st mode, with a field intensity of ~20 a.u., enabled stronger interaction with formalin, ideal for detecting larger changes, while the 4th mode's focused field improved precision. Comparisons with previous work confirmed the sensor's excellence, with a LoD of 0.127 to

0.230, showcasing its ability to detect trace formalin levels. Optimizing the back reflector and nanorings' thickness at 80 nm enhanced performance. With high sensitivity, reliable resolution, and a low detection limit, this sensor is a valuable tool for environmental monitoring, effectively identifying pollutants like formalin in water. It holds promise for protecting the environment and ensuring water safety. Future efforts could focus on practical testing and expanding its use to detect other chemicals, broadening its impact in environmental and medical fields.

Data availability

The datasets used and/or analyzed during the current study are available from the corresponding author upon reasonable request.

References

1. Puhar, J., Krajnc, D., Čuček, L. & Vujanović, A. Review and environmental footprint assessment of various formalin production pathways. *Journal of Cleaner Production* **377**, 134537 (2022).
2. Lyon, F. IARC monographs on the evaluation of carcinogenic risks to humans. *Some industrial chemicals* **60**, 389-433 (1994).
3. Liu, N. *et al.* Health effects of exposure to indoor formaldehyde in civil buildings: a systematic review and meta-analysis on the literature in the past 40 years. *Building and Environment* **233**, 110080 (2023).
4. La Torre, G., Vitello, T., Cocchiara, R. & Della Rocca, C. Relationship between formaldehyde exposure, respiratory irritant effects and cancers: a review of reviews. *Public Health* **218**, 186-196 (2023).
5. Muhammad, N. *et al.* Ion chromatography: A comprehensive review of sample preparation methods for analysis of halogens and allied nonmetals in critically challenging inorganic matrices. *Journal of Chromatography A* **1734**, 465311 (2024).
6. Wang, Z., Wang, W., Luo, A. Q. & Yuan, L. M. Recent progress for chiral stationary phases based on chiral porous materials in high-performance liquid chromatography and gas chromatography separation. *Journal of Separation Science* **47**, 2400073 (2024).
7. RANJAN, S., Chaitali, R. & SINHA, S. K. Gas chromatography–mass spectrometry (GC-MS): A comprehensive review of synergistic combinations and their applications

in the past two decades. *Journal of Analytical Sciences and Applied Biotechnology* **5**, 72-85 (2023).

8. Wekalao, J., Patel, S. K., Kumar, O. P. & Al-Zahrani, F. A. Machine learning optimized design of THz piezoelectric perovskite-based biosensor for the detection of formalin in aqueous environments. *Scientific Reports* **15**, 4498 (2025).

9. Hladová, M., Martinka, J., Rantuch, P. & Nečas, A. Review of spectrophotometric methods for determination of formaldehyde. *Vedecké Práce Materiálovotechnologickej Fakulty Slovenskej Technickej Univerzity v Bratislave so Sídlom v Trnave* **27**, 105-120 (2019).

10. Butt, M. A. Plasmonic sensor system embedded with orthogonal mode couplers for simultaneous monitoring of temperature and refractive index. *Plasmonics* **20**, 459-469 (2025).

11. Rahad, R. *et al.* A novel plasmonic MIM sensor using integrated 1× 2 demultiplexer for individual lab-on-chip detection of human blood group and diabetes level in the visible to near-infrared region. *IEEE Sensors Journal* **24**, 12034-12041 (2024).

12. Butt, M.A., M. Shahbaz, and R. Piramidowicz. Racetrack ring resonator integrated with multimode interferometer structure based on low-cost silica–titania platform for refractive index sensing application. *in Photonics*. **10**, 9-978 (2023).

13. Rakib, A., Muttaqi, M. R., Siddique, A. T. B., Siddique, M. A. B. & Sagor, R. H. Oxidation-resistant nanosensor: a label free, on-chip sensing approach of protein concentration, salinity, tissue classification. *Results in Physics* **53**, 106956 (2023).

14. Tian, J., Yu, S., Yan, W. & Qiu, M. Broadband high-efficiency surface-plasmon-polariton coupler with silicon-metal interface. *Applied Physics Letters* **95** (2009).

15. Rahad, R., Rakib, A., Haque, M. A., Sharar, S. S. & Sagor, R. H. Plasmonic refractive index sensing in the early diagnosis of diabetes, anemia, and cancer: an exploration of biological biomarkers. *Results in Physics* **49**, 106478 (2023).

16. Rakhshani, M. R. Ultra-narrowband light absorption with dual metamaterial ring resonator patches. *Optical Materials* **148**, 114826 (2024).

17. Mahadi, M. K., Rahad, R., Haque, M. A. & Nishat, M. M. Gated recurrent unit (GRU)-based deep learning method for spectrum estimation and inverse modeling in plasmonic devices. *Applied Physics A* **130**, 784 (2024).

18. Haque, M. A., Rahad, R. & Faruque, M. O. Optical computing at the subwavelength scale:<? TeX\break?> a multifunctional MIM plasmonic logic gate. *Applied Optics* **63**, 6364-6370 (2024).

19. Rahad, R., Mohsin, A. S., Bhuian, M. B. H. & Rahman, M. M. Graphene-metamaterial based tunable broadband polarization insensitive absorber for terahertz antenna design. *IEEE Access* **12**, 48654-48667 (2024).

20. Rakib, A., Siddique, A. T. B., Sakib, M. S., Faruque, M. O. & Sagor, R. H. A numerical analysis of a highly sensitive hexagonal plasmonic refractive index sensor. *Optics Communications* **530**, 129205 (2023).
21. Rahad, R., Rakib, A., Mahadi, M. K. & Faruque, M. O. Fuel classification and adulteration detection using a highly sensitive plasmonic sensor. *Sensing and Bio-Sensing Research* **40**, 100560 (2023).
22. Rahad, R. *et al.* A polarization independent highly sensitive metasurface-based biosensor for lab-on-chip applications. *Measurement* **231**, 114652 (2024).
23. Rahad, R., Joy, J. D., Rahman, M. S., Emon, M. J. H. & Haque, M. A. Miniaturized plasmonic sensor with dual-function capability for pressure and flow rate detection at subwavelength levels. *IEEE Sensors Journal* (2025).
24. Rahad, R. *et al.* Highly sensitive optically tunable transition metal nitride-based plasmonic pressure sensor with CMOS-compatibility at compact subwavelength dimensions. *IEEE Sensors Journal* **24**, 22271-22278 (2024).
25. Kabir, M. A. *et al.* High-performance demultiplexer-based lab-on-bio-chip sensor leveraging silicon photonics for point-of-care detection of hemoglobin and blood calcium ion levels. *Optics Express* **33**, 19788-19809 (2025).
26. Rahad, R. *et al.* An alternative plasmonic material-based CMOS-compatible temperature sensor. *Optics Communications* **569**, 130749 (2024).
27. Maier, S. A. *Plasmonics: fundamentals and applications*. Vol. 1 (Springer, 2007).
28. Singh, K. K., Kumar Mahto, S. & Sinha, R. A review: material characterization with metamaterial based sensors. *Sensor Review* **43**, 41-51 (2023).
29. Lee, Y., Kim, S.-J., Park, H. & Lee, B. Metamaterials and metasurfaces for sensor applications. *Sensors* **17**, 1726 (2017).
30. Palik, E. D. *Handbook of optical constants of solids*. Vol. 3 (Academic press, 1998).
31. Debnath, D. & Ghosh, S. K. Optical constants of noble metals at the nanoscale within the framework of the Drude free-electron conduction model: Implications for liquid crystal sensing. *ACS Applied Nano Materials* **5**, 1621-1634 (2022).
32. Saitta, L. *et al.* The effect of surface roughness on the performance of 3D printed surface plasmon resonance sensors for refractive index measurements. *The International Journal of Advanced Manufacturing Technology* **132**, 5503-5519 (2024).
33. Hyman, R., Stern, N. P. & Taflove, A. d'Alembert digitized: A wave pulse method for visualizing electromagnetic waves in matter and for deriving the finite difference time domain method for numerically solving Maxwell's equations. *American Journal of Physics* **89**, 164-171 (2021).

34. Parthasarathy, P. & Venkatesh, M. Developments in microfluidic integrated lab-on-chip devices for DNA biosensing towards unifying the emergence of nanobiosensor. *Biomedical Materials & Devices* **3**, 1104-1124 (2025).
35. Ren, Y., Duan, M., Guo, R. & Liu, J. Printed transformable liquid-metal metamaterials and their application in biomedical sensing. *Sensors* **21**, 6329 (2021).
36. Huang, Z., Droulias, S., Koschny, T. & Soukoulis, C. M. Mechanism of the metallic metamaterials coupled to the gain material. *Optics express* **22**, 28596-28605 (2014).
37. Zhang, J. *et al.* Plasmonic metasurfaces with 42.3% transmission efficiency in the visible. *Light: Science & Applications* **8**, 53 (2019).
38. Tang, Y., Zeng, X. & Liang, J. Surface plasmon resonance: an introduction to a surface spectroscopy technique. *Journal of chemical education* **87**, 742-746 (2010).
39. Mostufa, S., Paul, A. K. & Chakrabarti, K. Detection of hemoglobin in blood and urine glucose level samples using a graphene-coated SPR based biosensor. *OSA Continuum* **4**, 2164-2176 (2021).
40. Alsalman, O. *et al.* Design of split ring resonator graphene metasurface sensor for efficient detection of brain tumor. *Plasmonics* **19**, 523-532 (2024).
41. Danaie, M., Hajshahvaladi, L. & Ghaderpanah, E. A single-mode tunable plasmonic sensor based on an 8-shaped resonator for cancer cell detection. *Scientific Reports* **13**, 13976 (2023).
42. Abdi, G. & Bahador, H. High sensitivity and optimum design of LSPR-based sensors by coupled nano-rings for cancer detection. *Optics and Lasers in Engineering* **174**, 107975 (2024).
43. Bahador, H. & Heidarzadeh, H. Highly sensitive refractive index sensor by floating nano-particles in the solution for the detection of glucose/fructose concentration. *Optical and Quantum Electronics* **53**, 708 (2021).
44. Shi, B. *et al.* Compact slot microring resonator for sensitive and label-free optical sensing. *Sensors* **22**, 6467 (2022).
45. Mohammadi, M. & Seifouri, M. Numerical investigation of photonic crystal ring resonators coupled bus waveguide as a highly sensitive platform. *Photonics and Nanostructures-Fundamentals and Applications* **34**, 11-18 (2019).
46. Chorsi, H. T., Zhu, Y. & Zhang, J. X. Patterned plasmonic surfaces theory, fabrication, and applications in biosensing. *Journal of Microelectromechanical Systems* **26**, 718-739 (2017).
47. Vafapour, Z. *et al.* The potential of refractive index nanobiosensing using a multi-band optically tuned perfect light metamaterial absorber. *IEEE Sensors Journal* **21**, 13786-13793 (2021).

48. Taghipour, A. and H. Heidarzadeh. Design and analysis of highly sensitive LSPR-based metal–insulator–metal nano-discs as a biosensor for fast detection of SARS-CoV-2. in *Photonics*. **9**, 8-542 (2022).

Author Contributions

All authors contributed equally to this work.

Funding

This research received no external funding.

Additional information

Correspondence and requests for materials should be addressed to H.H.